Structural and dynamical properties of liquid Mg. An orbital-free molecular dynamics study

2009 J. Phys.: Condens. Matter 21 115106

(http://iopscience.iop.org/0953-8984/21/11/115106)

IOP Publishing Journal of Physics: Condensed Matter

J. Phys.: Condens. Matter **21** (2009) 115106 (11pp) doi:10.1088/0953-8984/21/11/115106

Structural and dynamical properties of liquid Mg. An orbital-free molecular dynamics study

S Şengül[1], D J González[2] and L E González[2]

[1] Physics Department, Trakya University, Edirne, Turkey
[2] Departamento de Física Teórica, Universidad de Valladolid, Valladolid, Spain

E-mail: david@liq1.fam.cie.uva.es

Received 4 December 2008, in final form 20 January 2009
Published 9 February 2009
Online at stacks.iop.org/JPhysCM/21/115106

Abstract

Several static and dynamic properties of liquid magnesium near melting have been evaluated by the orbital-free *ab initio* molecular dynamics method. The calculated static structure shows good agreement with recent experimental data, including an asymmetric second peak in the structure factor which has been linked to the existence of an important icosahedral short-range order in the liquid. As for the dynamic structure, we obtain collective density excitations with an associated dispersion relation which closely follows recent experimental results. Accurate estimates have also been obtained for several transport coefficients.

(Some figures in this article are in colour only in the electronic version)

1. Introduction

Molecular dynamics (MD) methods are a powerful technique to study the properties of liquid systems, and the last two decades have witnessed a large spread of the application of *ab initio* molecular dynamics methods (AIMD) based on the density functional theory (DFT) [1]. This theory allows calculation of the ground state electronic energy of a collection of atoms, for given nuclear positions, and also yields the forces on the nuclei via the Hellmann–Feynman theorem. It enables us to perform MD simulations in which the nuclear positions evolve according to classical mechanics whereas the electronic subsystem follows adiabatically. Most AIMD methods are based on the Kohn–Sham (KS) orbital representation of the DFT (KS-AIMD methods), which requires powerful computational resources, and this has imposed severe restrictions on the size of the systems and the simulation times. However, some of these constraints can be alleviated by the so-called orbital-free *ab initio* molecular dynamics (OF-AIMD) method, which by disposing of the electronic orbitals of the KS formulation provides a simulation method where the number of variables describing the electronic state is greatly reduced, enabling the study of larger samples (thousands of particles) and for longer simulation times (tens of ps).

This paper reports an *ab initio* molecular dynamics simulation on the static and dynamic properties of liquid magnesium (l-Mg) at thermodynamic conditions near its triple point. Mg is considered the simplest divalent metal. It belongs to the group of the alkaline-earth metals which is a group that has not attracted much attention, especially regarding the experimental work, possibly because of technical difficulties related to their high chemical reactivity and their gas adsorption ability [2]. Indeed, only a few properties have been measured, such as the static structure [3–5], density [6], sound velocity [7], electrical resistivity [8] and thermopower [9]. As a consequence, the theoretical work on the alkaline earths has also lagged behind that on the alkalis or the polyvalent metals. Recent experiments on l-Mg have determined its structure factors, both static [5] and dynamic [10]. It is precisely this recent availability of new experimental data which has prompted us to perform a comprehensive *ab initio* study of its static and dynamic properties.

The static structure factor of l-Mg was first measured by x-ray diffraction (XD) by Waseda [3, 4]; more recently, new XD and neutron scattering (NS) experiments have been performed aiming at a precise determination of the ion–valence electron structure factor [5], following initial efforts by Takeda *et al* [11]. Since neutrons scatter from nuclei and x-rays

from electrons, the difference between the structure factors measured with one or the other technique can provide some information about the electron distribution around ions, in particular for the valence electrons which are more delocalized than the tightly bound core electrons. As the difference between the structure factors is usually much smaller than their magnitude, large error bars are often found, and to reduce these uncertainties very precise measurements are required which, by the way, are becoming marginally possible due to the increased intensity of x-ray and neutron sources. Indeed, the recent, and more precise, XD data exhibit some discrepancies with respect to Waseda's. In particular, the height of the main peak of $S(q)$ is larger and the second peak also adopts an asymmetric form that departs from that predicted by the hard-sphere (HS) model which, incidentally, could accurately describe the shape of Waseda's $S(q)$. This specific shape of the second peak of $S(q)$ is similar to that found for several transition metals (Ni, Fe, Ti, Zr) [12, 13], and has been related to icosahedral (either ideal or distorted) short-range order that increases upon supercooling [14, 15], providing a nucleation barrier that inhibits crystallization [16]. Upon supercooling the asymmetry of the second peak increases and in fact a second subpeak develops. It is therefore interesting to analyse if this type of behaviour also occurs in the case of l-Mg.

Experimental investigations on the dynamic structure of l-Mg have been hampered by the high value of its adiabatic sound velocity ($\approx$4000 m s^{-1}), which stands close to the present limit of observability for inelastic neutron scattering (INS) due to the kinematic restrictions of this technique. However, these problems have been overcome by the use of inelastic x-ray scattering (IXS), and Kawakita *et al* [10] have recently used this technique to measure the dynamical structure of l-Mg at $T = 973$ K (which is about 50 K above the triple point). Specifically, the measurements by Kawakita *et al* have investigated the wavevector regions 0.2 Å^{-1} $\leqslant q \leqslant$ 3.11 Å^{-1} obtaining several dynamical features already observed in the liquid alkali metals, such as the existence of collective excitations up to q-values around $0.5q_p$ (where $q_p = 2.40$ Å^{-1} is the main peak position of $S(q)$), which exhibit a positive dispersion in the sound velocity with respect to the hydrodynamic value.

It is worth noting that recently the dynamic structure of liquid Fe, a system with icosahedral short-range order [12], has been studied by Hosokawa *et al* [17]. They analysed the results in terms of a theoretical model that includes three decay channels for the collective modes (thermal, structural and microscopic) and found some specific features of the structural terms at low q that behave different from those found in liquid alkali metals. This was tentatively attributed to the type of short-range order present in liquid Fe, and therefore it is interesting to study if such a behaviour is also observed in liquid Mg.

Most theoretical studies on l-Mg have addressed its thermodynamic and static structural properties, and the usual approach has been to characterize the liquid system by effective interatomic potentials constructed either empirically by fitting to experimental data or derived from some approximate theoretical model. Among those earliest semiempirical works, we mention reference [18] which basically resorted to the HS model with a packing fraction calculated within the framework of a variational theory based on the Gibbs–Bogoliubov inequality, to provide a fair estimate of the static structure of l-Mg at melting. Hafner and Jank [19] have followed a more fundamental approach to calculate some static and electronic properties of l-Mg near melting. They used an effective interatomic pair potential derived from the optimized pseudopotentials of Harrison [20], whereas the static structure was derived by classical molecular dynamics (CMD) simulations. The structural results showed good agreement with experiment and the calculated electronic density of states was basically free-electron-like. González and co-workers have used interatomic pair potentials derived from the neutral pseudoatom model [21–23] to calculate several static and dynamic properties of l-Mg. They used both CMD and liquid state theories [22, 24], yielding results in good agreement with the available experimental data. More recently, Bretonnet *et al* [25] have used an interatomic pair potential derived from the Fiolhais pseudopotential [26] along with CMD simulations to study several structural and thermodynamic properties for the alkali earths near melting.

Up to now, the only KS-AIMD calculation for l-Mg was performed by de Wijs *et al* [27, 28] more than ten years ago and it focused on the static and electronic properties for a thermodynamic state near the triple point. The calculation used 90 particles, a separable non-conserving pseudopotential and the local density approximation for the electronic exchange and correlation energy. Anta *et al* [29] performed OF-AIMD simulations of l-Mg which were focused on the static structure only. Both *ab initio* studies have provided accurate descriptions of the local liquid structure as compared to the then available XD data of Waseda, as well as valuable insights into the characteristics of the valence electronic charge densities. However, these studies did not address any dynamical properties. These were partially investigated by González *et al* in an OF-AIMD study using only 205 particles [23], in which only a few properties were considered mainly due to the lack of experimental data at that time. The study of these dynamic properties is the main subject of the present report which, to our knowledge, is the first comprehensive *ab initio* study on the dynamical properties of l-Mg.

2. Theory

A simple liquid metal is treated as a disordered array of N bare ions with valence Z, enclosed in a volume V, and interacting with $N_e = NZ$ valence electrons through an electron–ion potential $v(r)$. The total potential energy of the system can be written, within the Born–Oppenheimer approximation, as the sum of the direct ion–ion Coulombic interaction energy and the ground state energy of the electronic system under the external potential created by the ions, $V_{\rm ext}(\vec{r}, \{\vec{R}_l\}) = \sum_{i=1}^{N} v(|\vec{r} - \vec{R}_i|)$,

$$E(\{\vec{R}_l\}) = \sum_{i>j} \frac{Z^2}{|\vec{R}_i - \vec{R}_j|} + E_g[\rho_g(\vec{r}), V_{\rm ext}(\vec{r}, \{\vec{R}_l\})], \quad (1)$$

where $\rho_g(\vec{r})$ is the ground state electronic density and $\vec{R}_l$ are the ionic positions. According to DFT, the ground state

electronic density, $\rho_g(\vec{r})$, can be obtained by minimizing the energy functional $E[\rho]$, which can be written

$$E[\rho(\vec{r})] = T_s[\rho] + E_H[\rho] + E_{xc}[\rho] + E_{ext}[\rho] \quad (2)$$

where the terms represent, respectively, the electronic kinetic energy, $T_s[\rho]$, of a non-interacting system of density $\rho(\vec{r})$, the classical electrostatic energy (Hartree term), the exchange–correlation energy, $E_{xc}[\rho]$, for which we have used the generalized gradient approximation [30], and finally the electron–ion interaction energy, $E_{ext}[\rho]$. The electron–ion potential has been characterized by a local ionic pseudopotential, $v(r)$, constructed within DFT [31].

In the KS formulation [1], $T_s[\rho]$ is exactly evaluated by using single-particle orbitals, which imposes huge computational demands. This is ameliorated in the orbital-free approach [1, 31, 32] by using an explicit albeit approximate functional of the density for $T_s[\rho]$. We have used an average density model [31] that includes the von Weizsäker term and a Pauli term, $T_s = T_W + T_\alpha$,

$$T_W[\rho(\vec{r})] = \tfrac{1}{8}\int d\vec{r}\,|\nabla\rho(\vec{r})|^2/\rho(\vec{r}), \quad (3)$$

$$\begin{aligned} T_\alpha &= \tfrac{3}{10}\int d\vec{r}\,\rho(\vec{r})^{5/3-2\alpha}\tilde{k}(\vec{r})^2 \\ \tilde{k}(\vec{r}) &= (2k_F^0)^3\int d\vec{s}\;k(\vec{s})w_\alpha(2k_F^0|\vec{r}-\vec{s}|), \end{aligned} \quad (4)$$

where $k(\vec{r}) = (3\pi^2)^{1/3}\rho(\vec{r})^\alpha$, k_F^0 is the Fermi wavevector for mean electron density $\rho_e = N_e/V$, and $w_\alpha(x)$ is a weight function chosen so that both the linear response theory and Thomas–Fermi limits are correctly recovered. Further details are given in [31].

The local ionic pseudopotential, $v_{ps}(r)$, describing the ion–electron interaction has been constructed from first principles by fitting, within the same $T_s[\rho]$ functional, to the displaced electronic density induced by an ion embedded in a metallic medium as obtained in a KS-DFT calculation. Further details are given in [31] and we just note that the previous theoretical framework has already delivered an accurate description of static and dynamic properties of several bulk liquid metals and alloys [31, 33] as well as some liquid–vapour interfaces [34].

OF-AIMD simulations have been performed for l-Mg at a thermodynamic state near the triple point ($T = 953$ K). We have considered 2000 ions in a cubic cell with periodic boundary conditions and whose size was appropriate for an ionic number density $\rho_i = 0.038\,29$ Å^{-3} [4]. Given the ionic positions at time t, the electronic energy functional is minimized with respect to $\rho(\vec{r})$ represented by a single *effective orbital*, $\psi(\vec{r})$, defined as $\rho(\vec{r}) = \psi(\vec{r})^2$. The orbital is expanded in plane waves which are truncated at a cutoff energy, $E_{cut} = 13$ Ryd. The energy minimization with respect to the Fourier coefficients of the expansion is performed every ionic time step by using a quenching method which results in the ground state electronic density and energy. The forces on the ions are obtained from the electronic ground state via the Hellman–Feynman theorem, and the ionic positions and velocities are updated by solving Newton's equations, with the Verlet leapfrog algorithm with a timestep of 2.5×10^{-3} ps. In the simulations equilibration lasted 10 ps and the calculation of properties was made averaging over 50 ps.

During the simulation, we have evaluated several liquid static properties (pair distribution function, ion–ion and ion–valence electron static structure factors) as well as various dynamic properties, both single-particle ones (velocity autocorrelation function, mean square displacement) and collective ones (intermediate scattering functions, dynamic structure factors, longitudinal and transverse currents). The calculation of the time correlation functions (CFs) was performed by taking time origins every five time steps. Several CFs also have a dependence on the wavevectors $\mathbf{q}$ which, as our system is isotropic, depend on $q \equiv |\mathbf{q}|$ only.

3. Results

3.1. Static properties

We have already mentioned that the experimental determination of the distribution of valence electrons around nuclei, as quantified by the ion–valence electron structure factor, $S_{ie}(q)$, is a very difficult task. Nevertheless, it is a rather simple magnitude to compute in an *ab initio* simulation where the valence electrons are treated explicitly. It is directly obtained from the Fourier transform (FT) of the ion–valence electron distribution function, which can be computed in terms of the ionic positions and the selfconsistently obtained valence electron density. Another possible approach to a theoretical calculation of $S_{ie}(q)$ is the superposition approximation, where one considers that the system's valence electron density is the sum of spherically symmetric atomic-like valence electron densities attached to each ion in the system. In the KS-AIMD simulations of de Wijs *et al* [27, 28], it was shown that the superposition of the valence electron densities of a free Mg atom leads to poor results when compared to the selfconsistent ones, as observed in figure 1, reflecting the formation of bonds, metallic in this case. The reproducibility of this type of behaviour of the electronic properties by the (in principle) more approximate OF-AIMD methods would underpin their capability to tackle appropriately the electronic problem. Figure 1 depicts the OF-AIMD results for $S_{ie}(q)$ which show a remarkable similarity with the selfconsistent KS-AIMD result. Other OF-AIMD simulations of l-Mg, albeit using a different kinetic energy functional and a different pseudopotential [29], have also yielded good agreement with the KS-AIMD results, as seen in the figure. Finally, the $S_{ie}(q)$ obtained from the difference between the experimental NS and XD structure factors is also shown in figure 1. All the previous theoretical approaches reproduce well the trends in the experimental data and, in general, compare well with the experiments.

The simulations provide a direct evaluation of both the pair distribution function, $g(r)$, and the static structure factor, $S(q)$. The position of the main peak of $g(r)$ is customarily identified with the average nearest neighbour distance, which in the present OF-AIMD calculation stands at 3.10 Å, close to the experimental value [4] of ≈3.09 Å. The number of nearest

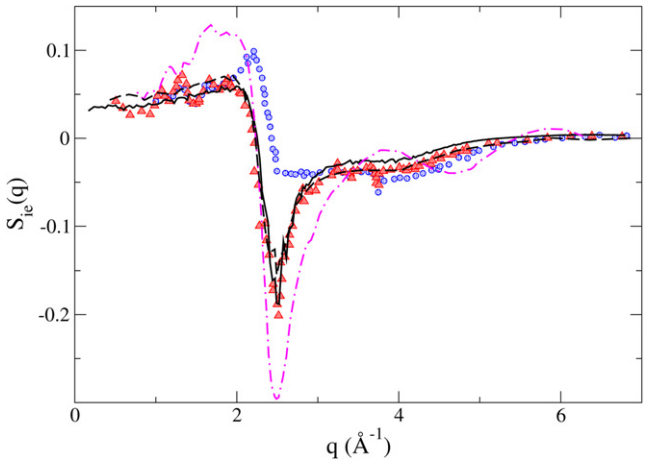

Figure 1. Ion–valence electron structure factor of l-Mg at 953 K. Continuous line: present OF-AIMD simulations. Triangles and circles: KS-AIMD simulation data from de Wijs *et al* [27, 28] corresponding to the selfconsistent density and to the superposition of free atom valence electron densities, respectively. Dashed line: OF-AIMD simulation results from Anta *et al* [29]. Dash–dotted line: experimental data of Tahara *et al* [5].

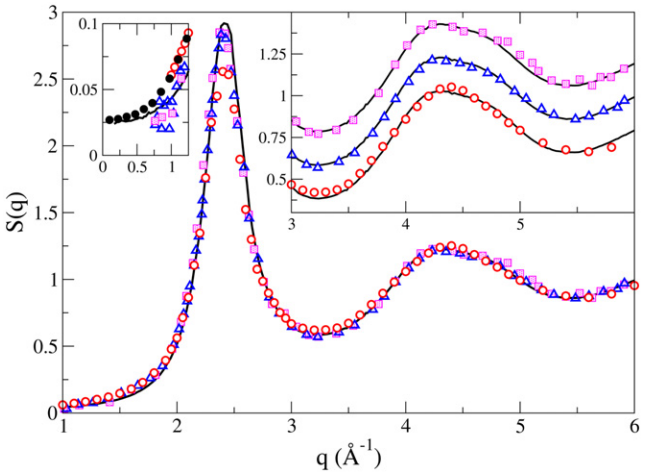

Figure 2. Static structure factor of l-Mg at 953 K. Open circles: experimental x-ray diffraction data from Waseda [4]. Triangles and squares: experimental XD and NS data at 973 K from Tahara *et al* [5]. Continuous line: OF-AIMD simulations. The left inset shows the low q behaviour, with full circles denoting small q XD measurements from Waseda. The right inset shows the second peak region, where Waseda's XD (Tahara's NS) data have been displaced downwards (upwards) by 0.2 units.

neighbours is obtained by integrating the radial distribution function (RDF), $4\pi r^2 \rho_i g(r)$, up to a distance r_m which is usually identified as the position of the first minimum in either the RDF or in $g(r)$ [35, 36]. Both choices usually lead to rather similar results, and in the present OF-AIMD based $g(r)$ we obtain that its first minimum is located at ≈4.35 Å whereas that of the RDF is at ≈4.23 Å, which lead to coordination numbers of ≈12.8 and 12.3 atoms/ions respectively.

The structure factor $S(q)$ is plotted in figure 2 along with the XD data of Waseda [4] and the new (XD and NS) diffraction data of Tahara *et al* [5]. The OF-AIMD based results coincide in every detail with the more recent data, particularly with respect to the height of the main peak and the asymmetric form of the second peak, as shown in the rightmost inset of figure 2. The other inset shows that in the small q region our results are closer to the new experiments than to the older ones.

Extrapolation of $S(q)$ to $q \to 0$ allows an approximate estimation of the isothermal compressibility, κ_T, by resorting to the relation $S(0) = \rho k_B T \kappa_T$. A least squares fit of $S(q) = s_0 + s_2 q^2$ to the calculated $S(q)$ for q-values up to 0.6 Å^{-1} yields the result $S(0) = 0.023 \pm 0.001$ and therefore a $\kappa_{T,\mathrm{OF-AIMD}} = 4.6 \pm 0.3$ (in 10^{-11} m^2 N^{-1} units) for $T =$ 953 K. We are unaware of any experimental measurement, but a recent estimate [37], based on experimental data for other thermodynamic magnitudes, suggests a value $\kappa_T = 5.05$. Unfortunately, a check on its accuracy is precluded by the lack of other estimates, either theoretical or experimental, for this magnitude.

An asymmetric shape of the second peak of $S(q)$ has already observed experimentally for several liquid transition metals and has been related to an important component of icosahedral local order. A first indication of such a type of short-range order is given by the positions of the maximum of the second peak of $S(q)$, q_2, and its 'shoulder', q_2', as compared to the position of the main peak. The corresponding values obtained for l-Mg are $q_2/q_p = 1.79$ and $q_2'/q_p \approx 1.97$, which are similar to those found for liquid Ti and Zr (1.76 and 1.92 respectively), or Ni (1.74 and 1.95), and not far from those corresponding to an ideal icosahedral environment in a curved space [38] of 1.71 and 2.04. A more detailed picture of the local order can be achieved by a common neighbour analysis of the system [39]. Each pair of neighbours is characterized by four indices, the first one indicating if the particles of the pair are first (1) or second (2) neighbours (i.e. if their separation is smaller or larger than 4.23 Å in this case). The second index indicates how many particles are common first neighbours of both particles in the pair, and the third index counts the number of first neighbour links among these shared neighbours. The fourth index discerns among different topologies (if they are feasible) that correspond to the same three first indexes. The relative abundance of each type of pairs can distinguish between different local structures like bcc, fcc, hcp or icosahedral. For instance, the abundance of 1551 pairs (corresponding to a local pentagonal bipyramid) points to a significant amount of ideal fivefold symmetry, as they show up in a centred perfect icosahedron whereas distorted icosahedra give rise to 1541 and 1431 pairs. Moreover, 1321 pairs appear in icosahedra too. So the sum of all these types of pairs is a measure of total (ideal and/or distorted) icosahedral short-range order. On the other hand, a local fcc environment is characterized by a large number of 1421 pairs, while a local hcp environment leads to high similar values of 1421 and 1422 pairs. Local bcc structure is finally characterized by large and similar numbers of 1441 and 1661 pairs, while an increase in 1661 pairs together with 1551 ones indicates a more complex polytetrahedral arrangement than icosahedra, in particular Frank–Kasper type polyhedra with 13 or more neighbours. Table 1 shows the results of

Table 1. Common neighbour analysis of the MD configurations of l-Mg at 953 K compared with several local structures.

Pairs	l-Mg	hcp	fcc	bcc
1551	0.14	0.00	0.00	0.00
1541	0.18	0.00	0.00	0.00
1431	0.23	0.00	0.00	0.00
1321	0.06	0.00	0.00	0.00
1421	0.05	0.50	1.00	0.00
1422	0.10	0.50	0.00	0.00
1301	0.01	0.00	0.00	0.00
1311	0.08	0.00	0.00	0.00
1331	0.00	0.00	0.00	0.00
1441	0.03	0.00	0.00	0.57
1661	0.03	0.00	0.00	0.43

the common neighbour analysis applied to the configurations generated in the OF-AIMD simulation run. Note that, in contrast to similar calculations by Jakse *et al* [15] for liquid Ni and Zr, we have not eliminated the thermal noise by finding the inherent structure (due to the cost of performing such optimization for a system with 2000 particles). Had we made this optimization, the number of distorted features would have diminished in favour of ideal ones. In this sense our analysis is more directly comparable to that of Kim and Kelton [14] who analysed experimental data of $S(q)$ through a reverse Monte Carlo procedure.

The fivefold symmetry dominates in l-Mg, as the sum of perfect and defective icosahedral structures amounts to 60% of the pairs, with the number of perfect ones smaller than those distorted probably due to the thermal disorder present in our calculations. There is also a 5–10% appearance of local hcp environments which is the phase in which Mg crystallizes. The amount of icosahedral short-range order is therefore smaller than in liquid Ni (where the total amounts to ca 80%), but quite similar to that in liquid Zr (around 60%) [15]. In this work we have not addressed the detailed calculations of the structure of undercooled l-Mg, but preliminary simulations down to 750 K show a development of a more pronounced shoulder in the second peak of $S(q)$ along with an increase both in the number of total and ideal pairs related to icosahedral short-range order (68%, almost half of them being 1551), together with a reduction of hcp related pairs. This would signal a high ability of l-Mg for supercooling which however has not been studied experimentally so far, at least to our knowledge. Note that this is the same behaviour as found in the liquid transition metals mentioned above [14, 15].

3.2. Dynamic properties

3.2.1. Collective dynamics. The intermediate scattering function, $F(q,t)$, embodies the information concerning the collective dynamics of density fluctuations over the length and time scales. It is defined as

$$F(q,t) = \frac{1}{N}\left\langle \left(\sum_{j=1}^{N} \mathrm{e}^{-\mathrm{i}\vec{q}\cdot\vec{R}_j(t+t_0)}\right)\left(\sum_{l=1}^{N} \mathrm{e}^{\mathrm{i}\vec{q}\cdot\vec{R}_l(t_0)}\right)\right\rangle, \quad (5)$$

where N is the total number of particles and $\vec{R}_j(t)$ is the position of the jth ion at time t. The time FT of the $F(q,t)$ into the frequency domain leads to the dynamic structure factor, $S(q,\omega)$, which has experimental relevance because it is directly related to the scattered intensity in the INS or IXS experiments. Another important magnitude associated with the density fluctuations is the current due to the overall motion of the particles, i.e.

$$\vec{j}(q,t) = \sum_{j=1}^{N} \vec{v}_j(t)\exp[\mathrm{i}\vec{q}\cdot\vec{R}_j(t)] \quad (6)$$

which is usually split into a longitudinal component, $\vec{j}_\mathrm{L}(q,t)$, parallel to $\vec{q}$, and a transverse component, $\vec{j}_\mathrm{T}(q,t)$, perpendicular to $\vec{q}$. Therefrom, the longitudinal, $C_\mathrm{L}(q,t)$, and transverse, $C_\mathrm{T}(q,t)$, current correlation functions are obtained as

$$C_\mathrm{L}(q,t) = \langle \vec{j}_\mathrm{L}(q,t)\cdot\vec{j}^{*}_\mathrm{L}(q,0)\rangle \quad (7)$$

$$C_\mathrm{T}(q,t) = \tfrac{1}{2}\langle \vec{j}_\mathrm{T}(q,t)\cdot\vec{j}^{*}_\mathrm{T}(q,0)\rangle. \quad (8)$$

The corresponding time FT gives the associated spectra, $C_\mathrm{L}(q,\omega)$ and $C_\mathrm{T}(q,\omega)$ respectively, with $C_\mathrm{L}(q,\omega) = \omega^2 S(q,\omega)$.

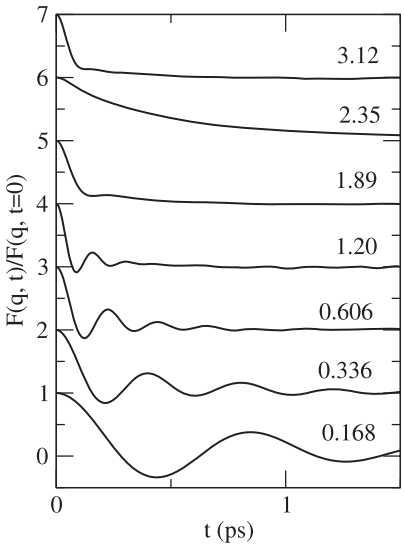

Figure 3. Calculated normalized intermediate scattering functions, $F(q,t)$, at several q-values (Å^{-1}) for l-Mg at $T = 953$ K.

Figure 3 shows the OF-AIMD calculated $F(q,t)$, for several q-values. The $F(q,t)$ exhibit an oscillatory behaviour up to $q \approx (3/5)q_p$, with the amplitude of the oscillations being stronger for the smaller q-values; indeed, this is the typical behaviour found, by both computer simulations [31, 40–42] and some theoretical models [43], for other simple liquid metals near their triple point. However, at these small q-values ($q \leqslant 0.5q_p$) the corresponding $F(q,t)$ show a weak diffusive component and the oscillations are rather marked around zero. The slow decay of $F(q,t)$ at $q \approx 2.35$ Å^{-1} is due to the so-called 'de Gennes narrowing' induced by the strong spatial correlations appearing at those q-values around q_p.

To extract additional information we have fitted the OF-AIMD calculated $F(q,t)$ to an analytical expression, based on the generalized hydrodynamic approximation, which

interpolates between the hydrodynamic ($q \to 0$) and the viscoelastic (accurate for $q \sim q_p$) model [44, 45], namely

$$\frac{F(q,t)}{S(q)} = A\exp(-at) + B\exp(-bt)\cos(\omega_0 t) + C\exp(-bt)\sin(\omega_0 t). \quad (9)$$

It has six q-dependent parameters and recovers the hydrodynamic $F(q,t)$ in the $q \to 0$ limit, with the coefficients behaving as

$$A \to \frac{\gamma - 1}{\gamma}, \qquad B \to \frac{1}{\gamma}, \qquad C \to \frac{d}{\gamma}q, \quad (10)$$

$$a \equiv D_T(q) \to D_T q^2, \qquad b \equiv \Gamma(q) \to \Gamma q^2, \qquad \omega_0 \to c_s q \quad (11)$$

where $\gamma = C_p/C_v$ is the ratio of specific heats, c_s is the adiabatic sound velocity, Γ is the sound attenuation constant, $D_T = \kappa_T/(\rho_i C_p)$ is the thermal diffusivity, κ_T is the thermal conductivity and d is a coefficient involving γ, Γ, c_s and D_T. The time FT of (9) gives the associated $S(q,\omega)$ whose analytical expression comprises the sum of a quasielastic Lorentzian peak and a pair of stretched Lorentzian inelastic peaks; moreover, when approaching the hydrodynamic limit they are changed into a diffusive peak at $\omega = 0$ (whose width is determined by D_T) along with two inelastic, propagating peaks centred at $\omega = \pm c_s q$ and half-width at half-maximum (HWHM) given by Γq^2.

We have already mentioned that for small q values the $F(q,t)$ show oscillations around zero, with a time decay which is ruled by the thermal diffusivity D_T (first term in the rhs of (9)). For a metallic system, D_T has both electronic and ionic contributions, with the former being much larger than the latter. However, the analysis of several calculations of this type [46] is consistent with incorporating in (9) only the part of D_T that is due to the ionic contribution. We have estimated D_T by fitting the OF-AIMD calculated $F(q,t)$ corresponding to the smallest q-values ($q \leqslant 0.6$ Å^{-1}) to the analytical expression (9). Within this q-range we have achieved a good fitting, yielding a value $D_T \sim 3.5(\pm 1) \times 10^{-3}$ cm^2 s^{-1}, which is two orders of magnitude smaller than the experimental value (which includes both ionic and electronic contributions) $D_T \sim 3.7 \times 10^{-1}$ cm^2 s^{-1} for l-Mg at melting [47]. We also quote that estimates of the ionic contribution to D_T in the liquid alkali metals near melting [48] range from 20.0×10^{-3} cm^2 s^{-1} (Li) to 3.0×10^{-3} cm^2 s^{-1} (Cs). As D_T rules the diffusive behaviour of the $F(q,t)$ at small q values, large D_T values imply a weak diffusive component which therefore is quickly overtaken by the oscillatory parts of the $F(q,t)$.

An alternative analysis of the data is provided through the modelling of the second order memory function of $F(q,t)$. The hierarchy of memory functions is most easily introduced by using Laplace transforms, $\tilde{f}(z) = \int_0^\infty f(t)\exp(-zt)\,\mathrm{d}t$, so that the first, $M(q,t)$, and second, $N(q,t)$, order memory functions of $F(q,t)$ are defined by

$$\tilde{F}(q,z) = \frac{F_0}{z + \tilde{M}(q,z)}, \qquad \tilde{M}(q,z) = \frac{M_0}{z + \tilde{N}(q,z)}. \quad (12)$$

The initial values of $F(q,t)$ and $M(q,t)$ are respectively $F_0 = F(q,t=0) = S(q)$ and $M_0 = M(q,t=0) = -F''(q,t=0)/F(q,t=0)$, where the prime denotes the time derivative. Within this formalism the hydrodynamic model corresponds to an $N(q,t)$ given by the sum of an instantaneous (Dirac-δ type) decay due to longitudinal viscosity and an exponential one due to thermal diffusivity. This model was generalized by substituting the viscous instantaneous decay by a viscoelastic exponential decay, although it was later found that two decay channels with different decay rates termed structural (slowly decaying) and microscopic (rapidly decaying) can give a better account of simulation and experimental data [44]. So, in the more general model $N(q,t)$ is given as a sum of three-exponential functions related to thermal, microscopic and structural relaxation. This model has been used in the analysis of IXS experimental measurements of the dynamic structure factor of several liquid metals [49], including recently liquid Fe [17]. In these studies the parameters related to thermal relaxation were taken from experimental thermophysical properties. However, the particular point to emphasize here is that in liquid Fe, as opposed to the liquid alkali metals, the contribution of the structural term to the kinematic longitudinal viscosity for finite q increases markedly with decreasing q. Even so, its contribution to the damping of the collective modes is negligible, because the timescale of the propagating mode is much shorter than the structural relaxation time, and therefore, from its point of view, the structure can be considered as frozen.

Taking into account the fact that the Laplace transform of an exponential function $a\exp(-bt)$ is $a/(z+b)$ and the structure of the hierarchy of memory functions it becomes easy to realize that if $N(q,t)$ is given by a sum of n exponentials, then $M(q,t)$ will be a sum of $n+1$ exponentials and $F(q,t)$ a sum of $n+2$ exponentials, which could however be either real or appear in complex conjugate pairs, thus including products of exponential functions and sines and cosines.

From the OF-AIMD results for $F(q,t)$ we have found that the corresponding second order memory function is well described by using only two exponential functions,

$$N(q,t) = a_s(q)\exp[-t/\tau_s(q)] + a_f(q)\exp[-t/\tau_f(q)], \quad (13)$$

i.e. a slowly decaying term and a rapidly decaying one. Correspondingly, $M(q,t)$ is given by a sum of one real and one complex conjugate pair of exponentials, and $F(q,t)$ by two real and one complex conjugate pair of exponentials.

From the fits to this model, which give similar accuracy to the ones in terms of the generalized hydrodynamic model, we have evaluated the q-dependence of the amplitudes and relaxation times involved. In figure 4 we plot the magnitudes of the terms $a_s(q)\tau_s(q)/q^2$ and $a_f(q)\tau_f(q)/q^2$, and we can observe a large increase in the slow contribution for small q. This behaviour is similar to that found in liquid Fe as analysed by Hosokawa *et al* from their experiments [17], and is in contrast to the behaviour found in several liquid alkali metals. This supports the idea that such an increase at low q may be related to the icosahedral short-range order present in both liquid Fe and Mg.

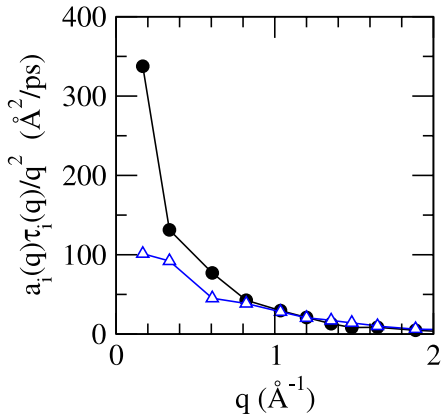

Figure 4. Values of $a_i(q)\tau_i(q)/q^2$ for the slowly decaying (circles) and rapidly decaying (triangles) terms of $N(q, t)$.

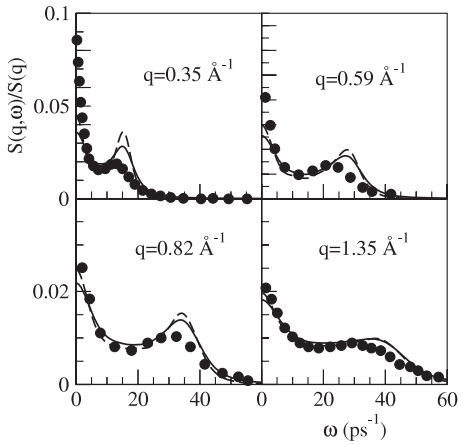

Figure 5. Dynamic structure factor, $S(q, \omega)$, at several q values, for l-Mg at $T = 953$ K. Full circles: experimental IXS data at 973 K [10]. Full and dashed lines: AIMD results for $q = 0.34, 0.61, 0.82$ and 1.36 Å^{-1}, after and before convolution with the experimental resolution function respectively.

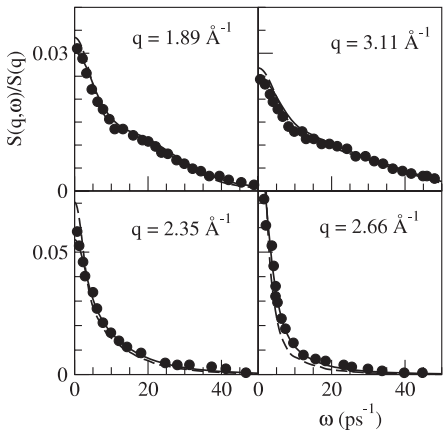

Figure 6. The same as in the previous graph but for $q = 1.89, 2.36, 2.66$ and 3.12 Å^{-1}.

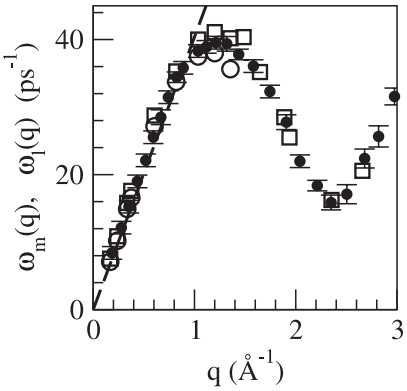

Figure 7. Dispersion relation for l-Mg at $T = 953$ K. Open circles: peak positions, $\omega_m(q)$, from the calculated $S(q, \omega)$. Open squares: peak positions, $\omega_l(q)$, from the maxima of the calculated longitudinal current, $C_l(q, \omega)$. Full circles: experimental $\omega_l(q)$ at $T = 973$ K from Kawakita *et al* [10]. Full line: linear dispersion with the hydrodynamic sound velocity, $v = 4050$ m s^{-1}.

The $S(q, \omega)$ has been calculated by a time FT of the $F(q, t)$ and figures 5 and 6 depict several $S(q, \omega)$ for a representative range of wavevectors. Up to $q \approx (3/5)q_p$, the $S(q, \omega)$ show well defined side peaks indicative of collective density excitations. Parenthetically we mention that the previous 205-particle OF-AIMD results by González *et al* [23] for those q values common with the present ones are quite similar, although the height of the quasielastic peak is now somewhat enhanced. A proper comparison with the measured IXS data [10] requires the prior convolution of the OF-AIMD calculated $S(q, \omega)$ with the experimental resolution function [10] as well as the inclusion of the detailed balance factor [44], even though this latter contribution has a negligible influence. On the other hand, the convolution with the experimental resolution function has the effect of diminishing the contact ($\omega = 0$) value as well as lowering and widening the side peaks. This is shown in figures 5 and 6 which depict the modified $S(q, \omega)$ which now show a better agreement with the experimental IXS data [10]. However, we notice that for small q values our calculated $S(q, \omega)$ still underestimate the quasielastic contribution.

From the positions of the side peaks, $\omega_m(q)$, the dispersion relation of the density fluctuations has been obtained and is depicted in figure 7 along with $\omega_l(q)$, which is the dispersion relation derived from the maxima of the longitudinal current correlation function, $C_l(q, \omega) = \omega^2 S(q, \omega)$. The figure also includes the experimental $\omega_l(q)$ data of Kawakita *et al* [10] at $T = 973$ K, as well as a line representing the dispersion of the hydrodynamic sound, whose slope gives the experimental [50] bulk adiabatic sound velocity $c_s = 4050$ m s^{-1} at $T = 953$ K.

In the hydrodynamic region, the slope of the dispersion relation curve gives a q-dependent adiabatic sound velocity, $c_s(q)$, which in the limit $q \to 0$ reduces to the bulk adiabatic sound velocity. Using the smallest three q-points of our calculated $\omega_m(q)$, we have performed a linear fitting obtaining an estimate for the bulk adiabatic sound velocity $c_s = 4200(\pm 150)$ m s^{-1} at $T = 953$ K. We also notice that the experimental dispersion relation data exhibit a *positive dispersion*, i.e. an increase of $\omega(q)$ with respect to the values predicted by the hydrodynamic adiabatic speed of sound, with a maximum located at $q \approx 0.6$ Å^{-1} and which amounts

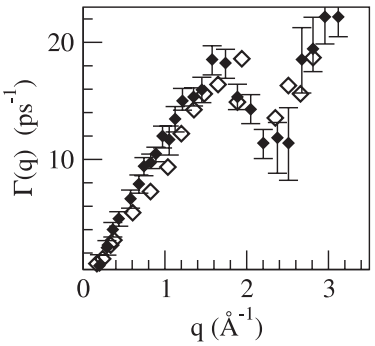

Figure 8. Full (open) diamonds with error lines: experimental (calculated) values for the HWHM, $\Gamma(q)$, of the inelastic peaks in l-Mg at $T = 953$ K.

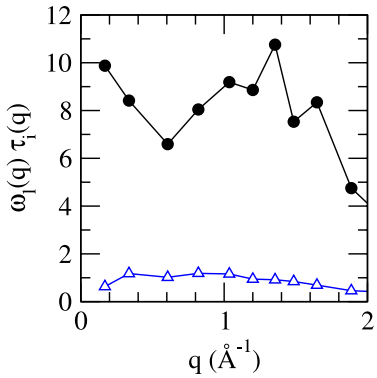

Figure 9. Products of the propagating frequency and each of the two relaxation times. Circles: slow term. Triangles: fast term.

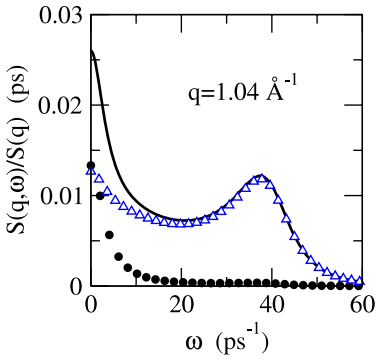

Figure 10. $S(q, \omega)$ for $q = 1.04$ Å^{-1} obtained from the two-exponential model for $N(q, t)$ (full line) along with its two contributions proportional to the strength of each exponential. Circles: slow term. Triangles: fast term.

to ≈8%. A similar magnitude of positive dispersion is also predicted by our calculated dispersion relations. We recall that the positive dispersion effect has already been experimentally found in several liquid metals such as the liquid alkali metals [51–53], Al [51] and Hg [54].

Another magnitude characterizing the collective density excitations is the HWHM of the inelastic peak, $\Gamma(q)$, which provides information on the lifetimes of the excitations. Figure 8 depicts the experimental data [10] for $\Gamma(q)$, which at small q values follow a quadratic law (hydrodynamic limit) but progressively depart from it as q increases. The figure also includes the calculated $\Gamma(q)$ obtained by fitting the OF-AIMD $F(q, t)$ to the analytical expression given by (9); this method was followed in order to disentangle the different contributions to the $F(q, t)$. In these calculations we find that in the first quasi-Brillouin zone, namely q-values up to $q_p/2 \approx 1.2$ Å^{-1}, the ratio $\Gamma(q)/\omega_l(q)$ varies between 0.18 and 0.32. For comparison, we mention that for a similar q-range the corresponding ratio varied within the interval (0.03–0.19) in l-Cs and (0.12–0.23) in l-Ga.

Returning to the two-exponential model for $N(q, t)$ (equation (13)) it is interesting to disentangle which of the two terms is mostly responsible for the damping of the propagating mode in $S(q, \omega)$. In figure 9 we show the products of the propagating frequency and the two relaxation times. It is clear that the long relaxation time is much larger than the typical time associated with the sound mode, leading to values of $\omega_l\tau$ around 10. This means that in the timescale of the density fluctuations the structure appears as frozen and hardly contributes to their damping. It is only for much smaller frequencies that the product becomes close to unity, and this means that a large part of the quasielastic peak in $S(q, \omega)$ is driven by this term. In contrast, the shorter relaxation time gives $\omega_l\tau_s$ values around unity, so that the fast term becomes responsible for the features of the inelastic peak.

These arguments can be reinforced by considering the explicit analytic expression of $S(q, \omega)$ obtained from the model through the relation $S(q, \omega) = \mathrm{Re}[\tilde{F}(q, z = \mathrm{i}\omega)]/\pi$. This leads to a rational function of ω with a denominator of degree eight and a numerator of second degree. Moreover, the numerator is given as a linear combination of the amplitudes of the exponentials of $N(q, t)$, so that $S(q, \omega)$ can be separated as a sum of contributions proportional to the strengths of each of the decaying channels. Such a decomposition is shown in figure 10 for $q = 1.04$ Å^{-1}, and reveals that the inelastic peak is almost exclusively obtained from the fast term while the slow one contributes only to the quasielastic line.

The transverse current correlation function, $C_t(q, t)$, is not associated with any measurable magnitude and can only be determined by means of computer simulations. It provides information on the shear modes and its shape evolves from a Gaussian, in both q and t, at the free-particle ($q \to \infty$) limit, towards a Gaussian in q and an exponential in t at the hydrodynamic limit ($q \to 0$), i.e.

$$C_t(q \to 0, t) = \frac{1}{\beta m} \mathrm{e}^{-q^2\eta|t|/m\rho}, \qquad (14)$$

where η is the shear viscosity coefficient, $\beta = (k_B T)^{-1}$ is the inverse of the temperature times the Boltzmann constant and m is the atomic mass. Whereas at both limits the corresponding $C_t(q, t)$ take positive values for all times, at intermediate q-values it may show a more complicated behaviour, including well defined oscillations within a limited q-range [31, 44, 45]. This is shown in figure 11 where we have depicted the calculated OF-AIMD results for several q-values. Notice that at the smallest q-value allowed by the simulation

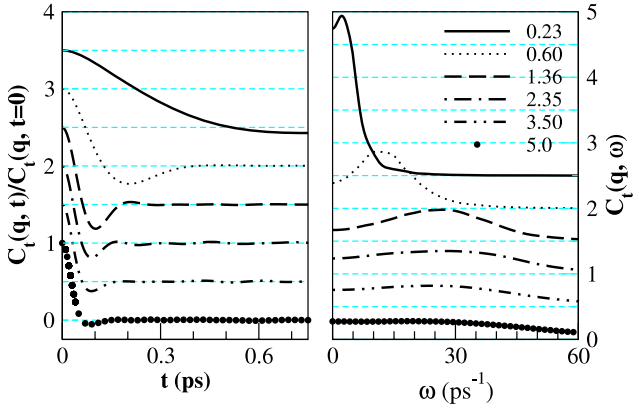

Figure 11. OF-AIMD transverse current correlation function, $C_t(q,t)$, and its spectra, $C_t(q,\omega)$, at several q-values (in Å^{-1}) for liquid Mg at $T = 953$ K.

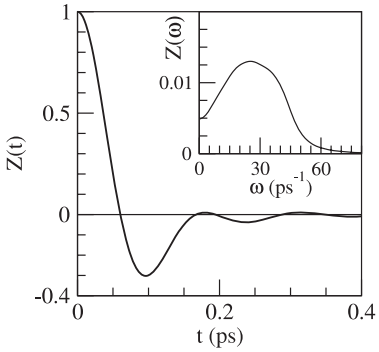

Figure 12. Normalized velocity autocorrelation function, $Z(t)$, of l-Mg at 953 K. The inset represents its power spectrum $Z(\omega)$.

($q = 0.168$ Å^{-1} $\approx 0.07 q_p$) the corresponding $C_t(q,t)$ already takes negative values, which by (14) means that it is already beyond the hydrodynamic regime. The associated spectrum, $C_t(q,\omega)$, is plotted in figure 11 and shows, for some intermediate q-range, an inelastic peak at nonzero frequency. This peak, which reflects the propagation of shear waves in the liquid, already exists at the smallest value reached by the simulation and remains up to $q \approx 2.5 q_p$. The associated peak frequency increases with q, takes a maximum value at $q \approx q_p$, and then decreases with increasing q while the corresponding $C_t(q,\omega)$ evolves towards a Gaussian shape. Indeed, a similar behaviour has already been reported for the alkali metals where the inelastic peak appears for $q \geqslant 0.07 q_p$ [44]. From the position of the maximum in the $C_t(q,\omega)$ a dispersion relation for the transverse modes, $\omega_t(q)$, can be obtained. We already mentioned that the q-value from where shear waves are supported (q_t) is smaller than the smallest value reached by the simulation. Assuming a linear dispersion in the vicinity of q_t, i.e. $\omega_t(q) \propto c_t(q - q_t)$ where c_t is the transverse velocity of sound, we obtain (using the smallest four q-values attained in the simulation) the following estimates: $q_t \approx 0.135$ Å^{-1} $\approx 0.055 q_p$ and $c_t \approx 2310$ m s^{-1}, much smaller than the longitudinal sound velocity.

From the calculated $C_t(q,t)$, we can estimate the shear viscosity coefficient, η, as follows [31, 55, 56]. The memory function representation of the $C_t(q,t)$,

$$\tilde{C}_t(q,z) = \frac{1}{\beta m}\left[z + \frac{q^2}{\rho m}\tilde{\eta}(q,z)\right]^{-1}, \qquad (15)$$

where the tilde denotes the Laplace transform, introduces a generalized shear viscosity coefficient, $\tilde{\eta}(q,z)$. The area under the normalized $C_t(q,t)$ gives $\beta m \tilde{C}_t(q, z = 0)$ wherefrom values for $\tilde{\eta}(q, z = 0)$ can be obtained and when extrapolated to $q = 0$ give the usual shear viscosity coefficient, η. The present OF-AIMD simulations give $\eta = 1.35 \pm 0.15$ GPa ps, whereas the available experimental data [57] at melting are $\eta_{\rm exp} = 1.31$ GPa ps which when extrapolated to $T = 953$ K gives an estimate $\eta_{\rm exp} \approx 1.16$ GPa ps.

3.2.2. Single-particle dynamics. The single-particle dynamic behaviour in liquid systems is usually analysed through the velocity autocorrelation function (VACF) of a tagged ion in the fluid, $Z(t)$, defined as

$$Z(t) = \langle \vec{v}_1(t)\vec{v}_1(0)\rangle / \langle v_1^2 \rangle \qquad (16)$$

which stands for the normalized VACF. The calculated $Z(t)$ is depicted in figure 12 and shows the usual shape characteristic of high density systems [31, 44] (i.e. the simple liquid metals near melting), which can be explained in terms of the so-called 'cage effect', namely, a tagged particle is enclosed in a cage formed by its adjacent neighbours. The $Z(t)$ exhibits an oscillatory behaviour with a distinct negative minimum at ≈0.1 ps followed by quickly decaying oscillations. Interestingly, a very similar shape with a minimum located at practically the same position is also displayed by the VACFs calculated by CMD [24, 25] and the KS-AIMD calculations of de Wijs *et al* [28].

The time FT of the $Z(t)$ gives its associated power spectrum $Z(\omega)$ which is also depicted in figure 12. It exhibits a broad maximum that reflects the oscillatory motions of the atoms/ions in the cage of their neighbours along with an incipient side peak shifted towards the higher frequencies, which has been previously related to the softness of the interatomic potential [58].

An estimate of the frequency at which a given atom/ion is vibrating within the cage [44, 45] can be achieved by a short time expansion $Z(t) = 1 - \omega_{\rm E}^2 t^2/2 \ldots$, where $\omega_{\rm E}$ is the so-called 'Einstein frequency' of the system. A short time fitting of our calculated $Z(t)$ gives $\omega_{\rm E} \sim 30.0$ ps^{-1} which is very close to the estimate $\omega_{\rm E} \sim 30.5$ ps^{-1} obtained by Kawakita *et al* [10] from their data on the q-dependent sound velocity. Finally, we mention that the CMD simulations by Alemany *et al* [24] yielded $\omega_{\rm E} \sim 31.7$ ps^{-1}.

The selfdiffusion coefficient, D, is readily obtained from either the time integral of $Z(t)$ or from the slope of the mean square displacement $\delta R^2(t) \equiv \langle |\vec{R}_1(t) - \vec{R}_1(0)|^2 \rangle$ of a tagged ion in the fluid, as follows:

$$D = \frac{1}{\beta m}\int_0^\infty Z(t)\,{\rm d}t; \qquad D = \lim_{t\to\infty} \delta R^2(t)/6t. \qquad (17)$$

Both routes for D lead to practically the same value, namely $D_{\mathrm{OF-AIMD}} = 0.51$ Å^2 ps^{-1}; unfortunately, no experimental data are available for comparison. Nevertheless, we mention that, using experimental data on other thermodynamic magnitudes, it has been hinted [50, 59] that $D_{\mathrm{exp}} = 0.56$–0.65 Å^2 ps^{-1} for l-Mg at $T = 923$ K. On the other hand, the CMD simulations of Alemany *et al* [24] yielded $D_{\mathrm{CMD}} = 0.665$ Å^2 ps^{-1} for l-Mg at $T = 953$ K, whereas the KS-AIMD of de Wijs *et al* [28] gave $D_{\mathrm{KS-AIMD}} = 0.50$ Å^2 ps^{-1} for l-Mg at $T = 1000$ K.

Within the context of the Brownian motion of a macroscopic particle of diameter d in a liquid of shear viscosity η, its selfdiffusion coefficient D is related to η through the Stokes–Einstein (SE) relation $\eta D = k_{\mathrm{B}}T/(2\pi d)$. Although approximate when applied to atoms/ions, this relation has sometimes been used to estimate η by identifying d with the main peak position of the $g(r)$. The present calculations give $d = 3.10$ Å, which combined with the value $D_{\mathrm{OF-AIMD}} = 0.51$ Å^2 ps^{-1} leads to $\eta = 1.33$ GPa ps, which is rather close to the OF-AIMD estimate and provides further reliability on the SE relation.

4. Conclusions

We have evaluated several static and dynamic properties of l-Mg close to the triple point. This has been done by using the orbital-free *ab initio* molecular dynamics method combined with a first-principles local pseudopotential constructed within the same framework.

Previous theoretical and simulation studies had already provided good descriptions of the local liquid structure and even some single-particle dynamical properties. Moreover, the *ab initio* studies of de Wijs *et al* [27, 28] and Anta *et al* [29] also provided some valuable insights into the properties of the valence electronic charge densities. However, the collective dynamical properties had only been partially addressed [23] and this has precisely been the main topic of the present report which, to our knowledge, is the first comprehensive *ab initio* study on the dynamical properties of l-Mg.

The intermediate scattering functions, $F(q,t)$, have at small q values a weak diffusive component and strong oscillations around zero. The associated dynamic structure factors, $S(q,\omega)$, show collective density excitations lasting for a similar range of q/q_p values as found for simple liquid metals near melting. There is a reasonable agreement with the experimental $S(q,\omega)$, although our calculations slightly overestimate the peak positions and for the smaller q values there is some underestimation for the intensity of the quasielastic contribution to the $S(q,\omega)$. Moreover, the calculated dispersion relation closely follows the existing experimental data.

The transverse current correlation functions, $C_t(q,t)$, exhibit clear oscillations around zero, and the associated spectra, $C_t(q,\omega)$, have inelastic peaks which reflect the presence of shear waves in the liquid. The calculated transport coefficients, namely selfdiffusion and shear viscosity, show a fair agreement with experiment and/or other *ab initio* calculations.

It is worth mentioning the accurate description of the valence electron–ion structure factor provided by the OF-AIMD method. Indeed, its results are practically coincident with those of the previous KS-AIMD simulations, which underlines the capability of the OF-AIMD method to deal correctly with the electronic problem.

The calculated static structure closely agrees with recent experimental data confirming an asymmetric second peak in the structure factor that is related to icosahedral short-range order of a degree similar to that of some transition metals like Zr, that is suggested to increase upon supercooling. This unveils a high potential of supercooling in l-Mg that could stimulate new experimental work. This type of ordering is accompanied by a large increase in the contribution of slow relaxation modes to the q-dependent generalized kinematic longitudinal viscosity for low q, in agreement with a recent analysis of experimental data for liquid Fe [17], so that both phenomena could indeed be related to each other. Further data along these lines would be helpful in clarifying this relationship. The overall good description achieved for several static and dynamic properties of l-Mg suggests that the OF-AIMD method may also reliably describe the undercooled state and address the natural question of how the short-range order and dynamic properties evolve in this undercooled region.

Acknowledgments

We are grateful to Professor N Jakse for fruitful discussions and for providing us with computer code related to the common neighbour analysis. SS acknowledges the EU Erasmus/Socrates programme that enabled a research stay in Spain. LEG and DJG acknowledge the support of the MCINN (FIS2008-02490/FIS), the EU FEDER programme and JCyL (VA068A06, GR120).

References

[1] Hohenberg P and Kohn W 1964 *Phys. Rev.* **136** B864
Kohn W and Sham L J 1965 *Phys. Rev.* **140** A1133
[2] Cook J G and Laubitz M J 1976 *Can. J. Phys.* **54** 928
[3] Waseda Y, Yokoyama K and Suzuki K 1974 *Phil. Mag.* **30** 1195
[4] Waseda Y 1980 *The Structure of Non-Crystalline Materials* (New York: McGraw-Hill)
[5] Tahara S, Fujii H, Yokota Y, Kawakita Y, Kohara S and Takeda S 2006 *Physica* B **385/386** 219
[6] Hiemstra S, Prins D, Grabielse G and van Zytveld J B 1977 *Phys. Chem. Liq.* **6** 271
[7] McAlister S P, Crozier E D and Cochram J F 1974 *Can. J. Phys.* **52** 1847
[8] van Zytveld J B, Enderby J E and Collings E W 1972 *J. Phys. F: Met. Phys.* **2** 73
[9] van Zytveld J B, Enderby J E and Collings E W 1973 *J. Phys. F: Met. Phys.* **3** 1819
[10] Kawakita Y, Hosokawa S, Enosaki T, Ohshima K, Takeda S, Pilgrim W C, Tsutsui S, Tanaka Y and Baron A Q R 2003 *J. Phys. Soc. Japan* **72** 1603
[11] Takeda S, Inui M, Tamaki S, Maruyama K and Waseda Y 1994 *J. Phys. Soc. Japan* **63** 1794
[12] Schenk T, Holland-Moritz D, Simonet V, Bellissent R and Herlach D M 2002 *Phys. Rev. Lett.* **89** 075507

[13] Lee G W, Gangopadhyay A K, Hyers R W, Rathz T J, Rogers J R, Robinson D S, Goldman A I and Kelton K F 2008 *Phys. Rev.* B **77** 184102
[14] Kim T H and Kelton K F 2007 *J. Chem. Phys.* **126** 054513
[15] Jakse N and Pasturel A 2003 *Phys. Rev. Lett.* **91** 195501
Jakse N and Pasturel A 2004 *J. Chem. Phys.* **120** 6124
Jakse N, Le Bacq O and Pasturel A 2007 *J. Non-Cryst. Solids* **353** 3684
[16] Kelton K F, Lee G W, Gangopadhyay A K, Hyers R W, Rathz T J, Rogers J R, Robinson M B and Robinson D S 2003 *Phys. Rev. Lett.* **90** 195504
[17] Hosokawa S, Inui M, Matsuda K, Ishikawa D and Baron A Q R 2008 *Phys. Rev.* B **77** 174203
[18] Umar I H and Young W H 1974 *J. Phys. F: Met. Phys.* **4** 525
Young W H 1992 *Rep. Prog. Phys.* **55** 1769
[19] Jank W and Hafner J 1990 *Phys. Rev.* B **42** 6926
[20] Harrison W A 1966 *Pseudopotentials in the Theory of Metals* (New York: Benjamin)
[21] González L E, González D J, Silbert M and Alonso J A 1993 *J. Phys.: Condens. Matter* **5** 4283
[22] González L E, Meyer A, Iñiguez M P, González D J and Silbert M 1993 *Phys. Rev.* E **47** 4120
[23] González L E, González D J and López J M 2001 *J. Phys.: Condens. Matter* **13** 7801
[24] Alemany M M G, Casas J, Rey C, Gonzalez L E and Gallego L J 1997 *Phys. Rev.* E **56** 6818
[25] Wax J F, Albaki R and Bretonnet J L 2000 *Phys. Rev.* B **62** 14818
[26] Fiolhais C, Perdew J P, Armster S Q, McLaren J M and Brajczewska M 1995 *Phys. Rev.* B **51** 14001
Fiolhais C, Perdew J P, Armster S Q, McLaren J M and Brajczewska M 1996 *Phys. Rev.* B **53** 13193 (erratum)
[27] de Wijs G A, Pastore A, Selloni A and van der Lugt W 1995 *Phys. Rev. Lett.* **75** 4480
[28] de Wijs G A 1995 *PhD Thesis* Rijksuniversiteit Groningen
[29] Anta J A, Jesson B J and Madden P A 1998 *Phys. Rev.* B **58** 6124
[30] Perdew J P 1991 *Electr Structure of Solids '91* ed P Ziesche and H Eschrig (Berlin: Academic) p 11
[31] González D J, González L E, López J M and Stott M J 2001 *J. Chem. Phys.* **115** 2373
González D J, González L E, López J M and Stott M J 2002 *Phys. Rev.* B **65** 184201
[32] Perrot F 1994 *J. Phys.: Condens. Matter* **6** 431
Smargiassi E and Madden P A 1994 *Phys. Rev.* B **49** 5220
Foley M and Madden P A 1996 *Phys. Rev.* B **53** 10589
[33] Canales M, González D J, González L E and Padró J A 1998 *Phys. Rev.* E **58** 4747
Blanco J, González D J, González L E, López J M and Stott M J 2003 *Phys. Rev.* E **67** 041024
González D J, González L E, López J M and Stott M J 2004 *Phys. Rev.* E **69** 031205
[34] González D J, González L E and Stott M J 2004 *Phys. Rev. Lett.* **92** 085501
González D J, González L E and Stott M J 2005 *Phys. Rev. Lett.* **94** 077801
González D J, González L E and Stott M J 2005 *J. Chem. Phys.* **123** 201101
[35] Cusak N E 1987 *The Physics of Structurally Disordered Matter* (Bristol: Hilger)
[36] McGreevy R L, Baranyai A and Ruff I 1986 *Phys. Chem. Liq.* **16** 47
[37] Singh R N, Arafin S and George A K 2007 *Physica* B **387** 344
[38] Sachdev S and Nelson D R 1984 *Phys. Rev. Lett.* **53** 1947
[39] Honeycutt J D and Andersen H C 1987 *J. Phys. C: Solid State Phys.* **91** 4950
[40] Torcini A, Balucani U, de Jong P H K and Verkerk P 1995 *Phys. Rev.* E **51** 3126
[41] Shimojo F, Hoshino K and Watabe M 1994 *J. Phys. Soc. Japan* **63** 141
[42] Kambayashi S and Kahl G 1992 *Phys. Rev.* A **46** 3255
Kahl G and Kambayashi S 1994 *J. Phys.: Condens. Matter* **6** 10897
[43] Casas J, González D J and González L E 1999 *Phys. Rev.* B **60** 10094
Casas J, González D J, González L E, Alemany M M G and Gallego L J 2000 *Phys. Rev.* B **62** 12095
[44] Balucani U and Zoppi M 1994 *Dynamics of the Liquid State* (Oxford: Clarendon)
[45] Hansen J P and McDonald I R 1986 *Theory of Simple Liquids* (London: Academic)
Boon J P and Yip S 1991 *Molecular Hydrodynamics* (New York: Dover)
[46] Chai J D, Stroud D, Hafner J and Kresse G 2003 *Phys. Rev.* B **67** 104205
[47] Touioukiam Y and Ho C 1973 *Thermophysical Properties of Matter* vol 10 *Thermal Diffusivity* (New York: IFI–Plenum)
[48] Cook J G and Fritsch G H 1985 *Handbook of Thermodynamic and Transport Properties of Alkali Metals* ed R W Ohse (Oxford: Blackwell) p 735
[49] Scopigno T, Ruocco G and Sette F 2005 *Rev. Mod. Phys.* **77** 881
[50] Iida T and Guthrie R I L 1988 *Physical Properties of Liquid Metals* (Oxford: Clarendon)
[51] Scopigno T, Balucani U, Ruocco G and Sette F 2000 *Phys. Rev.* E **63** 011210
[52] Sinn H and Burkel E 1996 *J. Phys.: Condens. Matter* **8** 9369
Sinn H, Sette F, Bergmann U, Halcoussis Ch, Krisch M, Verbeni R and Burkel E 1997 *Phys. Rev. Lett.* **78** 1715
[53] Pilgrim C, Hosokawa S, Saggau H, Sinn H and Burkel E 1999 *J. Non-Cryst. Solids* **250–252** 96
[54] Hosokawa S, Sinn H, Hensel F, Alatas A, Alp E E and Pilgrim C 2002 *J. Non-Cryst. Solids* **312–314** 163
[55] Palmer B J 1994 *Phys. Rev.* E **49** 359
[56] Balucani U, Brodholt J P, Jedlovszky P and Vallauri R 2000 *Phys. Rev.* E **62** 2971
[57] Shimoji M and Itami T 1986 *Atomic Transport in Liquid Metals* (Zurich: Trans. Tech. Publications)
[58] Canales M and Padró J A 1999 *Phys. Rev.* E **60** 551
González L E, González D J and Canales M 1996 *Z. Phys.* B **100** 601
[59] Iida T, Guthrie R I L and Tripathi N 2006 *Metall. Mater. Trans.* B **37** 559